Multi-proxy constraints on sapropel formation during the late Pliocene of central Mediterranean (southwest Sicily)

Julien Plancq[a]*[1], Vincent Grossi[a], Bernard Pittet[a], Carme Huguet[b2], Antoni Rosell-Melé[bc], Emanuela Mattioli[a]

[a] Laboratoire de Géologie de Lyon : Terre, Planètes, Environnement (UMR CNRS 5276), Université Lyon 1, Campus scientifique de la DOUA, 69622 Villeurbanne, France. E-mail addresses: vincent.grossi@univ-lyon1.fr (V. Grossi), bernard.pittet@univ-lyon1.fr (B.Pittet), emanuela.mattioli@univ-lyon1.fr (E. Mattioli)

[b] Institute of Environmental Science and Technology, Autonomous University of Barcelona, Edifici Cn-Campus UAB, 08193 Bellaterra, Catalonia, Spain. E-mail address : antoni.rosell@uab.cat (A. Rosell-Melé)

[c] Institució Catalana de Recerca i Estudis Avançats (ICREA), Barcelona, Catalonia, 08010, Spain. E-mail address: antoni.rosell@uab.cat (A. Rosell-Melé)

[*] Corresponding author : J. Plancq, Laboratoire de Géologie de Lyon, UMR 5276, CNRS, Université Lyon 1, Campus de la DOUA, Bâtiment Géode, 69622 Villeurbanne Cedex, France (e-mail address: plancq.julien@orange.fr; tel: +33 6 79 60 36 34).

[1] Present address : Laboratoire de Morphodynamique Continentale et Côtière (M2C), UMR CNRS 6143, Université Caen-Basse Normandie, Campus 1, 24 rue des tilleuls, Caen, France.

[2] Present address: Departamento de Geociencias, Universidad de los Andes, A.A. 4976. Bogotá, Colombia. E-mail address: m.huguet@uniandes.edu.co (C. Huguet).

Abstract

The late Pliocene (Piacenzian) in the Mediterranean region was punctuated by short-lived episodes of widespread deposition of organic-rich sedimentary layers known as sapropels. The causes of their formation remain a long-standing debate in the science community, and require disentangling the roles of climatic/oceanographic processes that triggered higher primary productivity or enhanced organic matter preservation. The lack of data, especially of sea temperatures at sufficient temporal resolution, is one of the main challenges to solve this debate.

Here, we present new organic geochemistry and micropaleontological data from the late Pliocene at Punta Grande/Punta Piccola sections (southwest Sicily) that allow untangling the mechanisms that favored the formation of two sapropel series (noted S and A) in the central Mediterranean area during this period. Sea surface (SSTs) and subsurface temperatures were estimated using three distinct organic geochemical proxies namely the alkenone unsaturation index ($U^{K'}_{37}$), the long-chain diol index (LDI) and the tetraether index (TEX_{86}). Reconstructed SSTs are relatively stable throughout the late Pliocene and ~4°C higher than modern Mediterranean SSTs, which is consistent with the climatic conditions inferred for this period from paleoclimate modeling. An increase in SST is, however, recorded by $U^{K'}_{37}$ and LDI proxies across each sapropel horizon, supporting that the two sapropel series S and A were formed during warmer climate conditions. The comparison of SST data with variations in accumulation rates of total organic carbon and lipid-biomarkers (alkenones, long-chain alkyl diols, archaeal and bacterial tetraethers), and with changes in calcareous nannofossil assemblages, indicates that the studied sapropels might have formed under different environmental conditions. The first series of sapropels (S), deposited between 3.1 and 2.8 Ma, is likely due to a better preservation of organic matter, induced by the development of a strong

thermohaline stratification of the water column and to oxygen-depleted bottom waters. Higher terrestrial input that occurred between 3.1 and 2.8 Ma may interestingly explain the large discrepancies observed between TEX_{86} and $U^{K'}_{37}$-LDI temperature values during this period. The second series of sapropels (A), deposited between 2.7 and 2.6 Ma, is more likely due to enhanced primary productivity in a weakly-stratified water column.

Keywords: Sapropels; Late Pliocene; Paleotemperatures; Calcareous nannofossils; Lipid-biomarkers.

1. Introduction

The late Pliocene (Piacenzian; 3.6-2.59 Ma) was characterized by the cyclic deposition of dark, organic matter-rich layers named sapropels in the Mediterranean Sea. Their formation is argued to be triggered by pulses of freshwater supply to the Mediterranean associated with the strengthening of the precessionally-controlled African monsoon (e.g., Béthoux, 1993; Foucault and Mélières, 2000; Combourieu Nebout et al., 2004), which led to enhanced primary productivity and organic matter export to marine sediments (Pedersen and Calvert, 1990), and/or enhanced water column stratification and improved organic matter preservation (e.g., Béthoux, 1993). Yet, the relative importance of increased export productivity *versus* organic matter preservation for the formation of sapropels is still uncertain.

The sapropels from the Punta Grande/Punta Piccola sections (southwest Sicily; Figure 1), considered as a reference for the cyclochronology of the middle Pliocene (Lourens et al., 1996), have been the subject of a number of chemical, mineralogical and palynological studies (e.g., Foucault and Mélières, 2000; Combourieu Nebout et al., 2004; Beltran et al., 2007). However, studies have been focused on a relatively limited number of sapropel layers (S104-S107). In addition, only a few studies have attempted to reconstruct sea surface

temperatures (SSTs) at high temporal resolution during the late Pliocene (Lourens et al., 1996; Herbert et al., 2015). Lourens et al. (1996) estimated SSTs at Punta Grande/Punta Piccola using oxygen isotopes and planktonic foraminifera assemblages (ratio warm *versus* cold taxa). In the Mediterranean, the interpretation of oxygen isotope data is, however, complicated by strong hydrological variability (e.g., Colleoni et al., 2012). More recently, Herbert et al. (2015) described a high-resolution reconstruction of Mediterranean SSTs based on the alkenone unsaturation index ($U^{K'}_{37}$; Prahl et al., 1988) to provide the first continuous record of Mediterranean for the late Pliocene-early Pleistocene (3.5-1.5 Ma).

Here, we have estimated marine temperatures from the Punta Grande/Punta Piccola section for the whole late Pliocene (3.6-2.6 Ma), using the indices $U^{K'}_{37}$, TEX_{86}, and long-chain diols or LDI (Prahl et al., 1988; Schouten et al., 2002; Rampen et al., 2012). The TEX_{86} is based on archaeal lipids (isoprenoidal glycerol dialkyl glycerol tetraethers, also known as isoprenoidal GDGTs) and is generally considered to reflect the annual mean SSTs (e.g., Schouten et al., 2013). However, several studies have argued that GDGT-based temperature proxy may, in some regions, better reflect subsurface temperatures rather than annual mean SSTs (e.g., Huguet et al., 2007). TEX_{86} is thus considered in the present study to integrate surface and subsurface water temperatures. We compared the reconstructed SSTs to changes in accumulation rates of calcareous nannofossils, total organic carbon (TOC) and lipid-biomarkers (alkenones, long-chain alkyl diols and isoprenoidal and branched GDGTs). Alkenones are produced by Haptophyte algae (Marlowe et al., 1990), long-chain alkyl diols by Eustigmatophyceae (1,13- and 1,15-diols) and/or *Proboscia* diatoms (1,14-diols) (Versteegh et al., 1997; Rampen et al., 2007), and GDGTs by aquatic Archaea (isoprenoidal GDGTs; Schouten et al., 2002) or terrestrial soil bacteria (branched GDGTs; Peterse et al., 2010). Changes in TOC, alkenone, long-chain diol, and isoprenoidal GDGT content, combined to calcareous nannofossil assemblages, provide reliable tracers of trophic

conditions in the upper part of the water column (e.g., Rampen et al., 2007; Schouten et al., 2013), while branched GDGT contents reflect terrestrial input into marine sediments (e.g., Hopmans et al., 2004). These new data are used to provide a comprehensive understanding of the environmental context in which sapropels were formed and to constrain the main mechanisms that favored their formation.

2. Materials and methods

2.1. Geological setting and sampling

The Capo Rossello composite section is located in the Caltanissetta basin (southwest of Sicily) and presents an excellent stratigraphy based on magnetic-isotopic data and on calcareous nannofossil record (Rio et al., 1990; Hilgen, 1991; Lourens et al., 1996). The Punta Grande and Punta Piccola sections represent the upper part of the Capo Rossello composite section and outcrop some 10 km west of Agrigento along the road from Porto Empedocle to the Rossello beach (Figure 1). The Punta Grande section and the lower part (first 14 m) of the Punta Piccola section are characterized by marls and marly limestones of the Trubi Formation (Hilgen, 1991). The uppermost part of the Punta Piccola section comprises regular alternations of grey marls and light-grey marly limestones of the Monte Narbone Formation, with the cyclical occurrence of dark laminated (sapropel) marl layers noted S101 to S112 and A1 to A5 (Hilgen, 1991; Lourens et al., 1996; Sprovieri et al., 2006).

A total of 61 samples were collected with an average sampling spacing of 80 cm in the Punta Grande and Punta Piccola sections, including the sapropel layers S101 to S109, S111, S112, A4, A4/5 and A5 (Figure 1). Both sections are beautifully exposed along the coast, with no tectonic disturbances or vegetation cover noticeable. Sampling was performed as deep as

125 possible beneath the surface (i.e. 10 to 30 cm) to collect fresh sediment and avoid the
126 weathered surface layer of the outcrops.
127 During the Pliocene, the studied sites were situated in an open marine slope-basin setting
128 in the Sicily sill, at a water depth of about 600-800 m (Sgarrella et al., 2012). According to the
129 age model of Lourens et al. (1996), the studied time interval spans the Piacenzian (late
130 Pliocene), from the Zanclean/Piacenzian boundary (3.6 Ma) to the Piacenzian/Gelasian
131 boundary coincident with the sapropel A5 mid-point (2.59 Ma), and comprises the Planktic
132 Foraminifera Zones MPL4B and MPL5A (Cita, 1975) and the Calcareous Nannofossil Zones
133 MNN 16a and MNN 16b-17 (Rio et al., 1990) (Figure 1). This age model was used to
134 determine the sedimentation rates in the studied sections.
135
136 **2.2. Calcareous nannofossil analyses**
137 Slides for quantitative counts of calcareous nannofossils were prepared following the
138 Random Settling method of Geisen et al. (1999). A small amount of dried sediment powder
139 (10 mg) was mixed with water (with basic pH, over-saturated with respect to calcium
140 carbonate) and the homogenised suspension was allowed to settle for 24 hours onto a cover
141 slide. The slide was dried and mounted on a microscope slide with Rhodopass. Four hundred
142 calcareous nannofossils (coccoliths and nannoliths) were counted in a variable number of
143 fields of views (between 15 and 30 according to the richness of the sample) using a polarizing
144 optical ZEISS microscope (magnification 1000x).
145 Absolute abundance of calcareous nannofossils per gram of sediment was calculated using
146 the formula:
147 $$X = (N \cdot V)/(M \cdot A \cdot H) \quad (1)$$
148 where X is the number of calcareous nannofossils per gram of sediment; N the number of
149 nannofossils counted in each sample; V the volume of water used for the dilution in the

settling device (475 cm^3); M the weight of powder used for the suspension (g); A the surface considered for nannofossil counting (cm^2); H the height of the water over the cover slide in the settling device (2.1 cm). Species-specific relative abundances (percentages) were also calculated from the total nannofossil content.

Taxonomic concepts adopted here followed the species classification according to Young and Bown (1997). The preservation of calcareous nannofossils (degree of etching and overgrowth) was estimated by optical and scanning electron microscopy observations, using the recommendations of Roth (1984).

2.3. Total Organic Carbon analyses

Sub-samples (ca. 50 mg of ground samples) were acidified with 2N HCl in pre-cleaned (combustion at 450°C) silver capsules until effervescence ceased, dried in an oven (50°C) and wrapped in tin foil before analyses. Duplicate Total Organic Carbon (TOC) analyses were performed with a Thermo FlashEA 1112 elemental analyzer using aspartic acid (36.09% of carbon) and nicotinamid (59.01% of carbon) as calibration standards. Repeated measurements of an in-house reference material (fine grounded low carbon sediment) were made to calibrate. Reproducibility achieved for duplicate analyses of all samples was better than 10% (coefficient of variation).

2.4. Lipid-biomarker analyses

Sixty-one samples were studied for alkenone content and 44 samples for long-chain diol and GDGT analyses. For each sampling interval, approximately 30 g of sediments was ground and extracted using sonication in Dichloromethane (DCM; 5 x 50 mL). Following evaporation of the solvent, the total lipid extract was separated into four lipid fractions of increasing polarity by chromatography over a Macherey-Nagel Chromabond® SPE (silica-

175 NH_2) cartridge with hexane, Hexane/DCM (3:1 v/v), DCM/acetone (9:1 v/v) and Methanol
176 (MeOH) as eluents, respectively. Each fraction was dried under nitrogen flow before
177 chromatography analyses.

178 Alkenones, contained in the second fraction (Hexane/DCM), were quantified by using a
179 gas chromatograph with a flame ionization detector (GC/FID) and hexatriacontane (*n*-C_{36}
180 alkane) as an internal standard (added in the sample before injection). GC/FID analyses were
181 performed on an HP-6890 Series gas chromatograph configured with an on-column injector
182 and an HP5 capillary column (30 m length, 0.32 mm internal diameter, 0.25 µm film
183 thickness). Helium was used as the carrier gas at constant flow (1.1 ml/min). The oven
184 temperature was programmed from 60°C (held for 1 min) to 130°C at 20°C/min, and then to
185 310°C (held for 20 min) at 4°C/min. The reproducibility achieved for duplicate alkenone
186 quantifications was estimated to be better than ±10% (coefficient of variation).

187 The global calibration of Müller et al. (1998), based on global core-top sediments (*n* =
188 370), was used to convert $U^{K'}_{37}$ values into SSTs.

$$U^{K'}_{37} = \frac{[C_{37:2}]}{[C_{37:2}] + [C_{37:3}]} \quad (2)$$

189 $$U^{K'}_{37} = 0.033(SST) + 0.044 \quad (3)$$

190 where $C_{37:2}$ and $C_{37:3}$ are di- and tri- unsaturated C_{37} alkenones, respectively
191 The standard error of the calibration is ± 1.5°C and analytical precision (1 σ) for duplicate
192 analyses is 0.2°C.

193 Following quantifications of alkenones, some alkenone fractions were reduced to the
194 corresponding unsaturated alcohols (alkenols) using $NaBH_4$ as described by Rontani et al.
195 (2011). This allows detecting small amounts of alkenones since alkenols display better
196 chromatographic characteristics.

Long-chain alkyl diols, isolated in the third fraction (DCM/acetone), were quantified by gas chromatography coupled to mass spectrometry (GC/MS) with electron impact ionization. Analyses were performed on a Agilent 6890N spectrometer interfaced to an HP6890 gas chromatograph equipped with an on-column injector and a DB-5MS capillary column (30 m x 0.25 mm x 0.25 µm). The oven temperature was programmed from 70°C (held for 0.5 min) to 130°C at 20°C/min, and then to 250°C at 5°C/min, finally reaching 300°C at 3°C/min (held for 30 min). The carrier gas (Helium) was maintained at 0.69 bar until 44 min and then programmed from 0.69 to 1.5 bar at 0.04 bar/min. To avoid potential biases due to co-elution, diols were quantified using specific fragment ions (see Versteegh et al., 1997) and hexatriacontane (*n*-C_{36} alkane) as an external standard. The reproducibility of the quantification was estimated to be ±10% (coefficient of variation).

The Long-chain Diol index (LDI) was calculated and converted into SSTs using the calibration of Rampen et al. (2012). This calibration is based on marine surface sediment data from different oceans (*n* = 162).

$$LDI = \frac{[C_{30}\text{-}1, 15]}{[C_{28}\text{-}1, 13] + [C_{30}\text{-}1, 13] + [C_{30}\text{-}1, 15]} \quad (4)$$

$$LDI = 0.033(SST) + 0.095 \quad (5)$$

where C_{30}-1,15, C_{28}-1,13, and C_{30}-1,13 indicate triacontane-1,15-diol (C_{30}-1,15), octacosane-1,13-diol (C_{28}-1,13), and triacontane-1,13-diol (C_{30}-1,13), respectively.

The standard error for the calibration is ± 2°C and analytical precision (1 σ) for duplicate analyses is 0.5°C. SST based on LDI could be calculated only in 34 samples, due to low abundances of C_{28}-1,13 diol in the other 10 samples.

The Diol index was also determined for the studied samples. This index, based on the ratio of C_{30} *vs.* C_{32} 1,15-diols, is sometimes used as a proxy for freshwater inputs (Versteegh et al., 1997).

The most polar fraction (4^{th}, MeOH) was prepared for GDGT analysis (GDGTs were only present in the 4^{th} fraction). A synthetic tetraether standard was added as surrogate to the fraction which was then re-dissolved in Hexane/Propanol (99:1 v/v), sonicated during 5 min and filtered using a 0.50 µl PTFE filter prior to injection. A Dionex P680 HPLC system coupled to a Thermo Finnigan TSQ Quantum Discovery Max quadrupole mass spectrometer with an APCI (Atmospheric Pressure Chemical Ionization) interface was used. The target compounds were separated using a Tracer Excel CN column (0.4 cm diameter, 20 cm length, 3 µm particle size; Teknokroma) equipped with a precolumn filter and a guard column. Samples were eluted with hexane/*n*-propanol at 0.6 mL/min. The amount of *n*-isopropanol was held at 1.5 % for 4 min, increased gradually to 5.0 % during 11 min, then increased to 10 % during 1 min and held at 10 % for 4 min, then decreased to 1.5 % during 1 min and held at 1.5 % for 9 min until the end of the run (Escala et al., 2009). Selected ion monitoring (SIM) was set to scan the five $[M+H]^+$ ions of the isoprenoid GDGTs and the $[M+H]^+$ ions of the three major branched GDGTs (Schouten et al., 2013). The reproducibility of the quantification is estimated to be ±10% (coefficient of variation).

The TEX_{86} was calculated and converted into sea (sub)surface temperature according to Kim et al. (2010). This calibration is based on core-top sediment data (n = 255) covering different oceanic locations, but excluding (sub)polar regions.

$$TEX^{H}_{86} = \log \left(\frac{[GDGT\text{-}2] + [GDGT\text{-}3] + [Cren']}{[GDGT\text{-}1] + [GDGT\text{-}2] + [GDGT\text{-}3] + [Cren']} \right) \quad (6)$$

$$T = 68.4 \times TEX^{H}_{86} + 38.6 \quad (7)$$

GDGT-1, GDGT-2 and GDGT-3 are isoprenoid GDGTs containing 1, 2, and 3 cyclopentane moieties, respectively. Cren' indicates crenarchaeol regio-isomer.

The standard error of temperature estimate is ± 2.5°C and analytical precision (1 σ) for duplicate analyses is 0.5°C.

2.5. Mass accumulation rates

The coccolith abundances, TOC and lipid-biomarker contents were expressed in accumulation rates to overcome the effects of a variable sedimentary dilution on nannofossil and organic matter concentrations (Figure 2). Accumulation rates (/cm^2/yr) were determined by multiplying the density of the calcite (2.7 g/cm^3) and the sedimentation rate (cm/yr) with the coccolith absolute abundances (specimens/g of sediment), organic matter content (g/g of sediment) and lipid-biomarker content (ng/g of sediment).

3. Results

3.1. Sedimentation rates

The sedimentation rate significantly increased at the top of the section (Figure 1). Between 3.6 and ~3 Ma (between 0 and 20.2 m), the sedimentation rate was of 3.4 cm/kyr but slightly increased (5.4 cm/kyr) between 3 and ~2.7 Ma (between 20.2 and 36.5 m). Between ~2.7 Ma and 2.6 Ma (between 36.5 and 48.4 m), the sedimentation rate significantly increased and reached values ca. twice as high than the previous interval (11.7 cm/kyr).

3.2. Calcareous nannofossil assemblages

Optical and scanning electron microscopy observations show that calcareous nannofossils are generally well preserved in all investigated samples, with very limited etching and overgrowth, both in sapropels and non-sapropel layers (Plate 1). Coccolith assemblages are well preserved and thus not biased by selective dissolution in the water column or diagenetic effects, as also reported in previous studies at Punta Grande/Punta Piccola (Sprovieri et al., 2006; Beltran et al., 2007).

The calcareous nannofossil accumulation rate (on average $61x10^6$ nannofossils/cm^2/yr) shows a significant stratigraphic trend across the Piacenzian. Between 3.6 and 3.1 Ma, accumulation rates are highly variable but a decreasing trend is observed (from ~$80x10^6$ to ~$40x10^6$ nannofossils/cm^2/yr; Figure 2a). Between 3.1 and 2.8 Ma, low accumulation rates are recorded ($40x10^6$ nannofossils/cm^2/yr on average), with even lower values in sapropels ($36x10^6$ nannofossils/cm^2/yr), but values progressively increase afterwards (between 2.8 and 2.6 Ma) reaching $165x10^6$ nannofossils/cm^2/yr at the top of the section (Figure 2a). Lower accumulation rates are observed in sapropels A4/5 and A5, but not in layer A4 probably due to the lower sampling resolution in this interval (Figure 2a).

Nannofossil assemblages are dominated by the genera *Reticulofenestra* and *Dictyococcites*, which account together for, on average, 70% of the total nannofossils (see Figure S1 in Supplementary data). *Reticulofenestra* is represented by the species *R. pseudoumbilicus*, *R. minutula* and *R. minuta*, and *Dictyococcites* by *D. antarcticus*, *D. hesslandii* and *Dictyococcites* spp. (specimens smaller than 3µm). The genus *Pseudoemiliania* is present in lower proportions (4% of the total nannofossils) and is only represented by the species *P. lacunosa*. Small *Gephyrocapsa* species (< 3µm) are also identified but these are too rare to be statistically significant (<0.1%). The oligotrophic nannolith *Discoaster* is present in low proportions (2% of the total nannofossil assemblage) but shows increased abundances (up to 10.5%) in most of the sapropels S101-S112. The ratio between the oligotrophic nannolith *Discoaster* (e.g., Flores et al., 2005) and the mesotrophic species *R. minutula* and *Dictyococcites* spp. (Flores et al., 2005) shows an increasing trend between 3.1 and 2.8 Ma and value peaks in the sapropel layers (Figure 2b). The remaining nannofossil taxa (*Coccolithus* spp., *Umbilicosphaera* spp., *Helicosphaera* spp., *Pontosphaera* spp., *Calcidiscus* spp., *Scyphosphaera* spp., *Sphenolithus* spp.) account for 25% of the total nannofossil assemblage on average (see Figure S1).

293

294 **3.3. Total organic carbon**

295 The total organic carbon content of the studied samples shows relatively low mean values
296 (0.4 wt.%) with higher values (0.6 wt.%) recorded in sapropel layers (except for S105, S108
297 and A5). TOC accumulation rates are relatively constant (0.0011 g/cm^2/yr) between 3.6 and
298 2.75 Ma, but they progressively increase upwards (from 2.75 to 2.6 Ma) with values reaching
299 0.0109 g/cm^2/yr at ~2.58 Ma (Figure 2c).

300

301 **3.4. Lipid-biomarkers**

302 Alkenone accumulation rates (comprising all alkenones identified) correlate relatively well
303 with that of TOC ($R^2 = 0.41$; $p < 0.0001$). The total accumulation rates are relatively low (3.7
304 ng/cm^2/yr in average), but higher values are recorded in sapropels, reaching up to 47.6
305 ng/cm^2/yr for sapropel S107 (Figure 2d). Alkenone accumulation rates remain relatively
306 constant (2.2 ng/cm^2/yr) between 3.6 and 2.8 Ma (except peaks observed in sapropels), but
307 they increase afterwards with values reaching 35.1 ng/cm^2/yr (Figure 2d). Five major
308 alkenones were present in all the samples, namely: heptatriacontatrien-2-one ($MeC_{37:3}$),
309 heptatriacontadien-2-one ($MeC_{37:2}$), octatriacontadien-3-one ($EtC_{38:2}$), octatriacontadien-2-one
310 ($MeC_{38:2}$) and nonatriacontatrien-3-one ($EtC_{39:2}$). The alkenone distribution differed in
311 sapropels S102, S107 and S112 with higher proportions of $EtC_{38:2}$ (and also of $EtC_{39:2}$) and
312 reduced proportions of $MeC_{37:2}$ (Figure 3). The $NaBH_4$ reduction of alkenones to the
313 corresponding alkenol silyl ethers (Rontani et al., 2011) sometimes allowed the identification
314 of three additional alkenones (under their alkenol form) yet with an unknown number of
315 unsaturation: one $EtC_{40:x}$ alkenone and two co-eluting Me- and $EtC_{41:x}$ alkenones (Figure 3).

316 Long-chain alkyl diols are also correlated to TOC ($R^2 = 0.67$; $p < 0.0001$) and alkenones
317 ($R^2 = 0.49$; $p < 0.0001$) but they show in general lower accumulation rates (1.2 ng/cm^2/yr)

(Figure 2d). Higher diol accumulation rates are recorded in sapropel layers, in particular in S101, S105, S107, S109, A4, A4/5 and A5 (with values up to 17.3 ng/cm^2/yr). The lowest accumulation rates of diols are observed between 3.6 and 3.1 Ma (0.1 ng/cm^2/yr). Both 1,14-diols, produced by *Proboscia* diatoms (Rampen et al., 2007) and 1,13- and 1,15-diols produced by Eustigmatophyceae (Versteegh et al., 1997) are present in the studied samples but the very low amount of 1,14-diols did not allow considering the two diol groups separately. The data thus represent the total pool of long-chain diols.

Total GDGTs show much lower accumulation rates (ca. $1 \cdot 10^{-2}$ ng/cm^2/yr) than phytoplanktonic lipids, but peaks are recorded at ~3.2 Ma, in sapropels S101, S107, S109, A4/5 and at ~2.61 Ma (with values up to $14.5 \cdot 10^{-2}$ ng/cm^2/yr) (Figure 2e). Isoprenoidal GDGT accumulation rates are ca. twice as high than that of branched GDGTs ($2 \cdot 10^{-2}$ ng/cm^2/yr and $1 \cdot 10^{-2}$ ng/cm^2/yr, respectively), except between ~3.03 and 2.8 Ma where accumulation rates of both GDGT pools are roughly similar ($0.38 \cdot 10^{-2}$ ng/cm^2/yr and $0.42 \cdot 10^{-2}$ ng/cm^2/yr for iGDGTs and brGDGTs, respectively) (Figure 2e).

In the present study, we used branched GDGT contents to track changes in soil terrestrial input rather than the Branched and Isoprenoid Tetraether (BIT) index. The BIT index was proposed as a proxy for the relative input of soil organic matter to coastal marine sediments, and has been used to estimate terrestrial organic matter input (e.g., Hopmans et al. 2004; Weijers et al., 2009). However, its application can be complicated by (i) high inputs of soil-derived crenarchaeol, (ii) *in situ* production of brGDGDTs in the aquatic environment or (iii) changes in archaea abundances in the water column through time. Thus, the BIT index is not just a terrigenous input indicator, as it also depends on the inputs of crenarchaeol closely linked to export productivity, and the quantification of branched GDGTs has been suggested to be a better terrestrial input indicator in some settings (e.g., Fietz et al., 2011).

343 **3.5. Marine temperatures**

344 Both LDI and $U^{K'}_{37}$ proxies attest for relatively stable SSTs throughout the late Pliocene,
345 with mean temperatures of 24.7°C and 25.6°C, respectively (Figure 4a and b). In spite of
346 these relatively long-term stable temperatures, an increase in SSTs is recorded by both
347 phytoplanktonic paleothermometers for most sapropels (mean temperatures of 25.1°C and
348 26.4°C for LDI and $U^{K'}_{37}$, respectively). This systematic increase seems more pronounced in
349 sapropels S101-S112 than in sapropels A4-A5 (Figure 4a and b).

350 Noticeably, the TEX_{86} temperatures, which may also reflect a subsurface signal (e.g.,
351 Huguet et al., 2007), show a pattern that is in line with SSTs reconstructed with the two other
352 organic proxies before (~3.4-3.1 Ma) and after (~2.8-2.6 Ma) the deposition of sapropels
353 S101-S112 (Figure 4c). During these periods, TEX_{86}, LDI and $U^{K'}_{37}$ temperature values are
354 very similar within the error range of the proxies (± 2.5°C for TEX_{86}), yielding an average
355 temperature of 24-25°C (Figure 4c). However, large discrepancies are observed among the
356 temperature proxies between 3.1- and 2.8 Ma, with a mean TEX_{86} temperature value of 19°C
357 that is substantially (about 6°C) cooler than $U^{K'}_{37}$ and LDI temperatures.

358

359 **4. Discussion**

360 **4.1. Temperature changes associated with sapropels**

361

362 Our results show that SSTs based on $U^{K'}_{37}$ and LDI systematically increased during
363 sapropel formation (Figure 4a and b). These would be in agreement with previous reports that
364 suggested higher temperatures during the deposition of these dark sedimentary layers based
365 on vegetation markers (Combourieu Nebout et al., 2004), alkenone distribution (Beltran et al.,
366 2007) and foraminifera assemblages (e.g., Sprovieri et al., 2006). Our estimates also agree
367 with those reported by Herbert et al. (2015) using $U^{K'}_{37}$ for the same location and the same

period, indicating that sapropels occurred in intervals of warmer SSTs. However, the record presented by Herbert et al. (2015) seems to show that SST variability was the same for both sapropel series (S101-112, A1-A5). The apparent less pronounced SST increase observed for sapropels A4-A5 in our study may be explained by a lower sampling resolution in this interval (Figure 4a).

The LDI is a recently developed paleothermometer that, so far, has only been used to reconstruct SSTs during the Quaternary period (e.g., Rampen et al., 2012). Here, LDI generally yields lower SST estimates than $U^{K'}_{37}$ (Figure 4a and b), but values stay within the error range of both proxies. In spite of a still incomplete and less robust calibration, our results highlight the potential use of the LDI proxy for pre-Quaternary periods.

The deposition of the present sapropels has been related to precession minima, implying hotter summer conditions in the Northern Hemisphere as a consequence of enhanced insolation (Hilgen, 1991; Lourens et al., 1996). Mean air temperatures (MAT) could be reconstructed from the present set of samples using the degree of methylation and cyclization of bacterial branched tetraethers (MBT'/CBT; Peterse et al., 2012; see Supplementary data and Figure S2). Our MAT estimates show concomitant changes with LDI and $U^{K'}_{37}$ sea temperatures between 2.8 and 2.6 Ma (Figure S2), which further supports that SST changes were related to higher MATs caused by higher insolation. Temperature changes seem to have affected the water column from the surface to the subsurface during the studied time interval as attested by the TEX_{86} index. Between 3.1 and 2.8 Ma, large discrepancies between TEX_{86} and $U^{K'}_{37}$-LDI temperature values are however observed. These discrepancies may hardly be explained by a selective degradation of GDGTs which appear relatively resilient (Kim et al., 2009). Instead, it might be caused by an input of terrestrial GDGTs biasing the marine TEX_{86} signal as it has been described previously in the Mediterranean Sea (Leider et al., 2010). This bias may be the result of enhanced freshwater supply as discussed below (section 4.2.1).

Reconstructed SSTs based on $U^{K'}_{37}$ and LDI are ~4°C higher than modern Mediterranean SSTs, which is consistent with the climatic conditions inferred for the late Pliocene from paleoclimate modeling (Haywood et al., 2002). Our estimates are however higher than values reported in the PRISM dataset, which is mainly based on quantitative analyses of planktonic foraminiferal faunas (Dowsett et al., 2012). Herbert et al. (2015) have argued that alkenones provide more accurate estimates of mean annual SST than those provided by planktonic foraminifera, although the differences observed between foraminiferal indices and alkenone SST estimates would merit more investigation. The systematic increase in SST observed in the S and A sapropel series is particularly interesting in the context of relatively stable temperatures characterizing the late Pliocene. This record may indeed highlight the role of seasonal insolation and land-sea heating contrasts in the formation of these organic-rich deposits by driving variations in rainfall over northern Africa and southern Europe (Herbert et al., 2015). Generally, the formation of Pleistocene and Holocene sapropels is not associated with a systematic temperature change (e.g., Emeis et al., 1998) contrary to the present sapropels. It is possible that for these Quaternary sapropels, SST was related to global ice volume changes, through cooling from inland glaciers and lowered snowlines in northern Mediterranean, and did not directly reflect warming due to higher insolation (Emeis et al., 1998) as in the present case. A major difficulty in comparing Punta Grande/Piccola's sapropels with those from the Pleistocene and Holocene derives from the fact that Quaternary sapropels were deposited in a context of wider climate variability, controlled by 41 kyr (obliquity) and/or 100 kyr (eccentricity) cycles related to oscillations of the northern ice sheets, whereas the 23 kyr (precession) cycle was dominant during the deposition of Pliocene sapropels (Hilgen, 1991).

4.2. Environmental changes and sapropel formation

4.2.1. Before the occurrence of first sapropel layers (3.6-3.1 Ma)

The highly fluctuating calcareous nannofossil accumulation rates, with higher proportions of mesotrophic species (such as *R. minutula*, *R. minuta* and *Dictyococcites* spp.) relative to the oligotrophic nannolith *Discoaster* (Figure 2a and b), indicate moderate but very fluctuating primary productivity in sea surface waters before the occurrence of sapropels S101-S112 (3.6-3.1 Ma). The relatively low TOC and lipid-biomarker accumulation rates recorded in this interval (Figure 2c and d) are in agreement with a relative nutrient-limited environment. Also, planktonic and benthic foraminifera indicate a relatively nutrient-limited environment, with abundance peaks (up to 30-60 %) of the oligotrophic planktonic species *Globigerinoides obliquus* and *Globigerinoides quadrilobatus* (Sprovieri et al., 2006). Abundance increases in oligotrophic species alternate with short periods of high proportion of hypoxic/eutrophic benthic foraminifera, although oxic/oligotrophic benthic species generally dominate in this interval (Figure 5b and c; Sgarrella et al., 2012). All these observations are in accordance with rather low export productivity before 3.1 Ma, with short periods of enhanced productivity (Figure 7a).

4.2.2. Sapropel layers S101-S112 (3.1-2.8 Ma)

The low nannofossil accumulation rates observed after 3.1 Ma (Figure 2a) indicates that sapropels S101-S112 were deposited during a time interval (3.1-2.8 Ma) characterized by oligotrophic conditions within the photic zone (Figure 7b). Higher proportions of the oligotrophic nannolith *Discoaster vs.* mesotrophic species (*R. minutula* and *Dictyococcites* spp.) are recorded in most sapropel layers (Figure 2b), further attesting for the development of oligotrophic sea surface waters. Van Os et al. (1994) argued that the nannofossil assemblage

observed in sapropel S102 from Punta Piccola was the result of enhanced dissolution, a phenomenon documented for some foraminifera and calcareous nannofossil species in eastern Mediterranean sapropels (e.g., Negri et al, 2003). According to these studies, *Discoaster* is thought to be more resistant to dissolution than *R. minutula* or *Dictyococcites* spp. In the present study, observations under optical and scanning electron microscopes show well-preserved calcareous nannofossils in both sapropel and non-sapropel layers of the Punta Grande/Punta Piccola composite section (Plate 1), with only a small degree of etching and/or overgrowth in agreement with previous studies (Sprovieri et al., 2006; Beltran et al., 2007). The decrease in abundance of *R. minutula* and *R. minuta* coupled to the increase in abundance of *Discoaster* is therefore more likely an ecological response to oligotrophic conditions rather than a bias induced by differential dissolution. Planktonic foraminifera assemblage data (Sprovieri et al., 2006) show overall low proportions of oligotrophic species but high proportions of the deep-dweller planktonic foraminifera *Globorotalia bononiensis* (Figure 5b), indicating increased nutrient concentrations with depth during the deposition of sapropels S101-S112. Benthic foraminifers are dominated by oxic/oligotrophic species between 3.1 and 2.8 Ma, but high proportions of hypoxic/eutrophic species are recorded in the sapropel layers. Overall oligotrophic conditions seem to have prevailed in the photic zone during this time interval, with an enhanced stratification of the water column during the deposition of the sapropels.

Interestingly, oligotrophy in sea surface waters during sapropel formation may be partly supported by a distinct alkenone profile observed in sapropels S102, S107 and S112, showing higher proportions of $EtC_{38:2}$ and $EtC_{39:2}$ alkenones coupled to lower proportions of $MeC_{37:2}$ alkenone (Figure 3). Culture experiments with the contemporary alkenone producers *Emiliania huxleyi* and *Gephyrocapsa oceanica* have indeed shown that, under nutrient depletion, the relative proportions of MeC_{37} alkenones decrease while those of Me- and EtC_{38}

and EtC_{39} increase (Prahl et al., 2003). Then, such a change in alkenone distribution might indicate stressing environmental conditions for alkenone producers during the deposition of sapropels S102, S107 and S112, further supporting oligotrophic conditions in surface Mediterranean waters during the deposition of these layers.

Concomitant with the oligotrophic marine conditions in the surface waters, higher contents of (terrestrial) branched GDGTs point to higher continental (river) inputs between 3.1 and 2.8 Ma (Figure 6b). The main transfer mechanism of branched GDGTs to marine environments is transport by rivers (Schouten et al., 2013). This observation is here supported by the so-called diol index, which indicates brackish-freshwater conditions (values lower than 68%) during the deposition of sapropels S106-S109 (Figure 6c). These results are in line with oxygen isotope data of planktonic foraminifera suggesting low-salinity conditions in surface waters, which have been attributed to increased freshwater input to the Mediterranean linked to the strengthening of the precessionally-controlled African monsoon (Tang and Stott, 1993; Beltran et al., 2007). Increased precipitation and continental runoff during the deposition of sapropels S104-108 have also been evidenced by i) higher proportions of smectite-chlorite (indicating fluvial erosion and discharge) relative to palygorskite (resulting from aeolian erosion of Saharan area) clay minerals (Foucault and Mélières, 2000) and ii) increased *Prasynophyceae* (freshwater algae) contents in palynomorph assemblages (Combourieu Nebout et al., 2004) (Figure 6d).

Enhanced freshwater supply between 3.1 and 2.8 Ma may explain the large discrepancies observed between TEX_{86} and $U^{K'}_{37}$-LDI temperature values (Figures 4 and 6a and b). Previous studies have shown a cold-bias of TEX_{86}-based temperatures occurring in coastal areas (e.g., Grauel et al., 2013). In particular, Leider et al. (2010) suggested that increased input of terrestrial isoprenoid GDGTs may bias TEX_{86} data towards lower temperatures, which may explain the anomalously low SST values recorded by TEX_{86} data in Mediterranean

493 coastal areas. Alternatively, higher freshwater input may have induced a deepening of the
494 chemocline in the water column, driving archaeal populations responsible for the TEX_{86}
495 signal to migrate towards cooler subsurface waters (Menzel et al., 2006; Huguet et al., 2007).
496
497 The oligotrophic sea surface water conditions and higher continental inputs, combined
498 with increased SSTs, attest for the development of an effective thermohaline stratification of
499 the water column and a lack of nutrient recycling in surface waters during formation of
500 sapropels S101-S112 (Figure 7c). This thermohaline stratification would account for the
501 enhanced preservation of organic matter in sapropels, because it would have promoted
502 reduced ventilation at the water-sediment interface through the weakening of the
503 Mediterranean anti-estuarine circulation. Although complete anoxic conditions probably did
504 not develop in bottom waters at Punta Grande/Punta Piccola, benthic foraminifera
505 assemblages still point to hypoxic conditions during sapropel deposition (Sgarrella et al.,
506 2012; Figure 5c), which would explain the systematic higher TOC and alkenone/diol contents
507 recorded in these layers (Figure 2c and d). Stratford et al. (2000) have shown that, even with a
508 modest reduced ventilation of the bottom waters, a weakened Mediterranean anti-estuarine
509 circulation could decrease bottom water oxygenation sufficiently to enhance organic carbon
510 deposition.
511
512 *4.2.3. Sapropel layers A4-A5 (2.7-2.6 Ma)*
513 The progressive increase in phytoplanktonic biomarkers and TOC accumulation rates from
514 2.8 Ma (Figure 2c and d), and the concomitant slight increase in the proportions of eutrophic
515 planktonic foraminifera species *Neogloboquadrina acostaensis* (Figure 5b; Sprovieri et al.,
516 2006), suggest that sapropels A4-A5 were deposited during a progressive enhancement of
517 export primary productivity (Figure 7d). This change in nutrient availability in the water

column may reflect paleoceanographic changes linked to the intensification of Northern Hemisphere glaciations occurring at ~2.7 Ma (Hilgen, 1991; Lourens et al., 1996; Sprovieri et al., 2006). The associated glacio-eustatic sea level falls would have increased continental weathering, as attested by an increase in accumulation rates, thus favoring primary productivity at Punta Piccola.

Contrary to sapropels S101-S112, in A4-A5 layers, the relative abundance of oligotrophic nannofossil species (Figure 2a and b) does not increase but higher proportions of hypoxic/eutrophic benthic foraminifers (Sgarrella et al., 2012; Figure 5c) are recorded. This testifies for enhanced export production from the surface to the deep water during the formation of this sapropel series. Sgarrella et al. (2012) argued for an increase in river runoff during the deposition of sapropels A4-A5, in particular for sapropel A5. Fluctuating increases of the oligotrophic planktonic foraminifera *G. quadrilobatus* and of *G. obliquus* together with peaks of eutrophic species *N. acostaensis* indeed suggest periods of surface water stratification and more eutrophic subsurface waters (Figure 5b). This is however not in accordance with the proportions of branched GDGTs and the Diol index that we observe and that do not evidence higher terrestrial input between 2.8 and 2.6 Ma (Figure 6b and c). In addition, very low proportions of the deep-dweller planktonic foraminifera *G.bononiensis* are recorded during this interval (Figure 5b). These observations, without excluding sea surface stratification, rather tend to indicate lower terrestrial inputs during the deposition of sapropels A4-A5 than during the formation of sapropels S101-S112 (3.1-2.8 Ma).

Our data further suggest that the deposition of sapropels A4-A5 was more likely controlled by enhanced primary productivity as attested by the higher alkenone/diol contents of these layers (Figure 2c and d). Still, a thermohaline stratification cannot be completely excluded, especially because an increase in SST is also recorded during the deposition of sapropels A4-

A5 (Figure 7e), but the temperature-driven effect would be less effective than for sapropels S101-S112.

4.2.4. Comparison between the two sapropel series

Our data, coupled with previously reported studies, show that the mechanism responsible for the formation of sapropels A4-A5 may be distinct from that of sapropels S101-S112. While these latter were likely formed primarily thanks to a better preservation of organic matter (Figure 7c), the formation of sapropels A4-A5 was probably due to enhanced primary productivity (Figure 7e).

Our results appear contradictory to previous works that suggested that sapropels S101-S112 of the Punta Piccola section were due to enhanced primary productivity (e.g., Van Os et al., 1994; Sgarrella et al., 2012). Our dataset provide, however, evidence of effective thermohaline stratification during the deposition of sapropels S101-S112. It is possible that this stratification resulted in a deepening of the nutricline, as it has been suggested to occur during the formation of Zanclean and Late Pleistocene sapropels (Castradori, 1998; Incarbona et al., 2011). This hypothesis is further supported by the increased abundances of the deep-dweller planktonic foraminifera *Globorotalia bononiensis* observed in sapropels S101-S112 (Figure 5b) (Sprovieri et al., 2006). By refurnishing nutritive elements, a deep nutricline might have then led to an effective downwards export of organic matter from the intermediate part of the water column. During the deposition of sapropels A4-A5, no significant increase in the proportions of *G. bononiensis* is recorded, which suggests a less effective thermohaline stratification. It is possible that enhanced organic matter input to bottom waters have induced oxygen-depleted bottom waters through the degradation of organic matter by bacterial activity, as attested by higher proportions of hypoxic/eutrophic benthic foraminifers (Figure

5b). Enhanced organic matter input could have thus also promoted a better preservation of organic matter.

These observations would support the idea that, for both Pliocene sapropel series, carbon concentration in sapropels may have been influenced by both preservation and primary productivity (Gallego-Torres et al., 2011). The formation of each sapropel series was however driven by a distinct dominant mechanism, namely preservation for sapropels S101-S112 and productivity for sapropels A4-A5.

5. Conclusion

Cyclic, orbitally-driven temperature increases related to the African monsoon system promoted water column stratification in the Mediterranean during the relatively stable climate conditions of the late Pliocene. This mechanism, coupled to the development of a more or less permanent low-salinity surface layer due to increased continental runoff, certainly played a role in the formation of sapropels S101-S112 at Punta Grande/Punta Piccola. This indeed enhanced the stratification of the water column and improved organic matter preservation. Our multi-proxy study however demonstrates that Pliocene sapropel formation cannot be exclusively explained by organic matter preservation. Enhanced primary productivity in a weakly-stratified water column indeed better explains the formation of sapropels A4-A5. In summary, both sapropel series may be linked to enhanced organic matter preservation and primary productivity, but a distinct mechanism appears mainly responsible of each sapropel series.

The present work highlights the necessity of using a multi-proxy approach to obtain a more comprehensive picture of the environmental context in which sapropels can form.

Acknowledgements

We would like to thank two anonymous reviewers for their constructive comments that helped to significantly improve the quality of the manuscript. We warmly thank Antonio Caruso (University of Palermo, Italy) and Agata Di Stefano (University of Catania, Italy) for their help during field trip. We are also grateful to Laurent Simon (University of Lyon, France) and Julie Lattaud for help with TOC and diol analyses respectively. A travel scholarship to J. Plancq from the European Association of Organic Geochemist (EAOG) is gratefully acknowledged.

References

Beltran, C., de Rafélis, M., Minoletti, F., Renard, M., Sicre, M.-A., Ezat, U., 2007. Coccolith $\delta^{18}O$ and alkenone records in middle Pliocene orbitally controlled deposits: high frequency temperature and salinity variations of sea surface water. Geochem. Geophys. Geosyst., 8 (5), doi:10.1029/2006GC001483.

Béthoux, J.P., 1993. Mediterranean sapropel formation, dynamic and climatic viewpoints. Oceanol. Acta 16, 127–133.

Castradori, D., 1998. Calcareous nannofossils in the basal Zanclean of the eastern Mediterranean sea: remarks on paleoceanography and sapropel formation. In: Robertson, A.H.F., Emeis, K.-C., Richter, C., Camerlenghi, A. (Eds.), Proceedings of the Ocean Drilling Program Scientific Results, Volume 160. College Station, Texas, Ocean Drilling Program, pp. 113–123.

615 Cita, M.B., 1975. The Miocene-Pliocene boundary. History and definition, in: Saito, T.,
616 Burckle, L.H. (Eds.), Late Neogene Epoch Boundaries. Spec. Publ., 1. Micropaleontol.
617 Press, pp. 1–30.
618 Colleoni, F., Masina, S., Negri, A., Marzocchi, A., 2012. Plio-Pleistocene high–low latitude
619 climate interplay: a Mediterranean point of view. Earth Planet. Sci. Lett. 319, 35–44.
620 Combourieu-Nebout, N., Foucault, A., Mélières, F., 2004. Vegetation markers of
621 palaeoclimate cyclical changes in the Pliocene of Punta Piccola (Sicily, Italy).
622 Palaeogeogr. Palaeoclim. Palaeoecol. 214 (1-2), 55–66, doi:
623 10.1016/j.palaeo.2004.07.021.
624 Dowsett, H.J., Robinson, M.M., Haywood, A.M., Hill, D.J., Dolan, A.M., Stoll, D.K., Chan,
625 W.-L., Abe-Ouchi, A., Chandler, M.A., Rosenbloom, N.A., Otto-Bliesner, B.L., Bragg,
626 F.J., Lunt, D.J., Foley, K.M., Riesselman, C.R., 2012. Assessing confidence in Pliocene
627 sea surface temperature to evaluate predictive models. Nat. Clim. Change 2, 365–371,
628 doi: 10.1038/nclimate1455.
629 Emeis, K.-C., Schulz, H.-M., Struck, U., Sakamoto, T., Doose, H., Erlenkeuser, H., Howell,
630 M., Kroon, D., Paterne, M., 1998. Stable isotope and alkenone temperature records of
631 sapropels from sites 964 and 967: constraining the physical environment of sapropel
632 formation in the eastern Mediterranean sea. In: Robertson, A.H.F., Emeis, K.-C., Richter,
633 C., Camerlenghi, A. (Eds.), Proceedings of the Ocean Drilling Program Scientific
634 Results, Volume 160. College Station, Texas, Ocean Drilling Program, pp. 309–331.
635 Escala, M., Fietz, S., Rueda, G., Rosell-Melé, A., 2009. Analytical considerations for the use
636 of the paleothermometer Tetraether Index (86) and the Branched vs Isoprenoid Tetraether
637 Index regarding the choice of cleanup and instrumental conditions. Analytical Chemistry
638 81, 2701-2707.

639 Fietz, S., Martínez-Garcia, A., Huguet, C., Rueda, G., Rosell-Melé, A., 2011. Constraints in
640 the application of the Branched and Isoprenoid Tetraether index as terrestrial input proxy.
641 J. Geophys. Res. 116, doi:10.1029/2011JC007062.
642 Flores, J.-A., Sierro, F.J., Filippelli, G.M., Bárcena, M.Á., Pérez-Folgado, M., Vázquez, A.,
643 Utrilla, V., 2005. Surface water dynamics and phytoplankton communities during
644 deposition of cyclic late Messinian sapropel sequences in the western Mediterranean.
645 Mar. Micropaleontol. 56, 50-79.
646 Foucault, A., Mélières, F., 2000. Palaeoclimatic cyclicity in central Mediterranean Pliocene
647 sediments: the mineralogical signal. Palaeogeogr. Palaeoclimatol. Palaeoecol. 158 (3-4),
648 311–323, doi: 10.1016/S0031-0182(00)00056-0.
649 Gallego-Torres, D., Matinez-Ruiz, F., Meyers, P.A., Paytan, A., Jimenez-Espejo, F.J., Ortega-
650 Huerta, M., 2011. Productivity patterns and N-fixation associated with Pliocene-
651 Holocene sapropels: paleoceanographic and paleoecological significance. Biogeosciences
652 8 (2), 415–431, doi: 10.5194/bg-8-415-2011.
653 Geisen, M., Bollmann, J., Herrle, J.O., Mutterlose, J., Young, J.R., 1999. Calibration of the
654 random settling technique for calculation of absolute abundance of calcareous
655 nannoplankton. Micropaleontology 45 (4), 437–442.
656 Grauel, A.-L., Leider, A., Goudeau, M.-L.S., Müller, I.A., Bernasconi, S.M., Hinrichs, K.-U.,
657 de Lange, G.J., Zonneveld, K.A.F., Versteegh, G.J.M., 2013. What do SST proxies really
658 tell us? A high-resolution multiproxy ($U^{K'}_{37}$, TEX^{H}_{86} and foraminifera $\delta^{18}O$) study in the
659 Gulf of Taranto, central Mediterranean Sea. Quat. Sc. Reviews 73, 115–131.
660 Haywood, A.M., Valdes, P.J., Sellwood, B.W., 2002. Magnitude of climate variability during
661 middle Pliocene warmth: a palaeoclimate modelling study. Palaeogeogr. Palaeoclimatol.
662 Palaeoecol. 188 (1-2), 1–24, doi: 10.1016/S0031-0182(00)00056-0.

663 Herbert, T.D., Ng, G., Peterson, L.C., 2015. Evolution of Mediterranean sea surface
664 temperatures 3.5-1.5 Ma: regional and hemispheric influences. Earth Planet. Sci. Lett.
665 409, 307–318.
666 Hilgen, F.J., 1991. Extension of the astronomically calibrated (polarity) time scale to the
667 Miocene/Pliocene boundary. Earth Planet. Sci. Lett. 107 (2), 349–368, doi:
668 10.1016/0012-821X(91)90082-S.
669 Hopmans, E.C., Weijers, J.W.H., Schefuß, E., Herfort, L., Sinninghe Damsté, J.S., Schouten,
670 S., 2004. A novel proxy for terrestrial organic matter in sediments based on branched and
671 isoprenoid tetraether lipids. Earth Planet. Sci. Lett. 224, 107–116.
672 Huguet, C., Schimmelmann, A., Lourens, L.J., Sinninghe Damsté, J.S., Schouten, S., 2007. A
673 study of the TEX_{86} paleothermometer in the water column and sediments of the Santa
674 Barbara Basin, California. Paleoceanography 22 (3), PA3203, doi:
675 10.1029/2006PA001310.
676 Incarbona, A., Ziveri, P., Sabatino, N., Salvagio Manta, D., Sprovieri, M., 2011. Conflicting
677 coccolithophore and geochemical evidence for productivity levels in the Eastern
678 Mediterranean sapropel S1. Mar. Micropaleontol. 81 (3-4), 131–143, doi:
679 10.1016/j.marmicro.2011.09.003.
680 Kim, J.-H., Huguet, C., Zonneveld, K.A.F., Versteegh, G.J.M., Roeder, W., Sinninghe
681 Damsté, J.S., Schouten, S., 2009. An experimental field study to test the stability of lipids
682 used for the TEX_{86} and $U^{K'}_{37}$ palaeothermometers. Geochim. Cosmochim. Acta 73 (10),
683 2888–2898, doi: 10.1016/j.gca.2009.02.030.
684 Kim, J.-H., van der Meer, J., Schouten, S., Helmke, P., Willmott, V., Sangiorgi, F., Koç, N.,
685 Hopmans, E.C., Sinninghe Damsté, J.S., 2010. New indices and calibrations derived from
686 the distribution of crenarchaeal isoprenoid tetraether lipids: Implications for past sea

surface temperature reconstructions. Geochim. Cosmochim. Acta 74 (16), 4639–4654, doi: 10.1016/j.gca.2007.12.010.

Leider, A., Hinrichs, K.-U., Mollenhauer, G., Versteegh, G.J.M., 2010. Core-top calibration of the lipid-based $U^{K'}_{37}$ and TEX_{86} temperature proxies on the southern Italian shelf (SW Adriatic Sea, Gulf of Taranto). Earth Planet. Sci. Lett. 300 (1-2), 112–124, doi: 10.1016/j.epsl.2010.09.042.

Lourens, L.J., Antonarakou, A., Hilgen, F.J., Van Hoof, AA.M., Vergnaud-Grazzini, C., Zachariasse, W.J., 1996. Evaluation of the Plio-Pleistocene Astronomical Timescale. Paleoceanography 11 (4), 391–413, doi: 10.1029/96PA01125.

Marlowe, I.T., Brassell, S.C., Eglinton, G., Green, J.C., 1990. Long-chain alkenones and alkyl alkenoates and the fossil coccolith record of marine sediments. Chem. Geol. 88 (3-4), 349–375, doi: 10.1016/0009-2541(90)90098-R.

Menzel, D., Hopmans, E.C., Schouten, S., Sinninghe Damsté, J.S., 2006. Membrane tetraether lipids of planktonic Crenarchaeota in Pliocene sapropels of the eastern Mediterranean Sea. Palaeogeogr. Palaeoclimatol. Palaeoecol. 239 (1-2), 1–15, doi: 10.1016/S0031-0182(00)00056-0.

Müller, P. J., Kirst, G., Ruhland, G., von Storch, I., Rosell-Melé, A., 1998. Calibration of the alkenone paleotemperature index $U^{K'}_{37}$ based on core-tops from the eastern South Atlantic and the global ocean (60°N–60°S). Geochim. Cosmochim. Acta 62, 1757– 1772.

Negri, A., Morigi, C., Giunta, S., 2003. Are productivity and stratification important to sapropel deposition? Microfossil evidence from late Pliocene insolation cycle 180 at Vicra, Calabria. Palaeogeogr. Palaeoclimatol. Palaeoecol. 190, 243–255, doi: 10.1016/S0031-0182(02)00608-9.

Pedersen, T.F., Calvert, S.E., 1990. Anoxia vs. productivity: What controls the formation of organic-carbon-rich sediments and sedimentary rocks? Am. Assoc. Petr. Geol. Bull. 74, 454–466.

Peterse, F., Nicol, G.W., Schouten, S., Sinninghe Damsté, J.S., 2010. Influence of soil pH on the abundance and distribution of core and intact polar lipid-derived branched GDGTs in soil. Org. Geochem. 41 (10), 1171–1175, doi: 10.1016/j.orggeochem.2010.07.004.

Peterse, F., van der Meer, J., Schouten, S., Weijers, J.W.H., Fierer, N., Jackson, R.B., Kim, J.-H., Sinninghe Damsté, J.S., 2012. Revised calibration of the MBT-CBT paleotemperature proxy based on branched tetraether membrane lipids in surface soils. Geochim. Cosmochim. Acta 96, 215–229, doi: 10.1016/j.gca.2012.08.011.

Prahl, F.G., Muehlhausen, L.A., Zahnle, D.L., 1988. Further evaluation of long-chain alkenones as indicators of paleoceanographic conditions. Geochim. Cosmochim. Acta 52 (9), 2303–2310, doi: 10.1016/0016-7037(88)90132-9.

Prahl, F.G., Wolfe, G.V., Sparrow, M.A., 2003. Physiological impacts on alkenone paleothermometry. Paleoceanography 18 (2), 1025, doi: 10.1029/2002PA000803.

Rampen, S.W., Schouten, S., Wakeham, S.G., Sinninghe Damsté, J.S., 2007. Seasonal and spatial variation in the sources and fluxes of long chain diols and mid-chain hydroxy methyl alkanoates in the Arabian Sea. Org. Geochem. 38 (2), 165–179, doi: 10.1016/j.orggeochem.2006.10.008.

Rampen, S.W., Willmott, V., Kim, J.-H., Uliana, E., Mollenhauer, G., Schefuß, E., Sinninghe Damsté, J.S., Schouten, S., 2012. Long chain 1,13- and 1,15-diols as a potential proxy for palaeotemperature reconstruction. Geochim. Cosmochim. Acta 84, 204–216, doi: 10.1016/j.gca.2012.01.024.

733 Rio, D., Sprovieri, R., Thunell, R., Vergnaud Grazzini, C., Glaçon, G., 1990. Pliocene-
734 Pleistocene paleoenvironmental history of the Western Mediterranean: a synthesis of
735 ODP Site 653 results. Proc. ODP Sci. Res. 107, 695–704.
736 Rontani, J.-F., Wakeham, S.G., Prahl, F.G., Vaultier, F., Volkman, J.K., 2011. Analysis of
737 trace amounts of alkenones in complex environmental samples by way of $NaBH_4/NaBD_4$
738 reduction and silylation. Org. Geochem. 42 (11), 1299–1307, doi:
739 10.1016/j.orggeochem.2011.09.004.
740 Roth, P.H., 1984. Preservation of calcareous nannofossils and fine-grained carbonate particles
741 in mid-Cretaceous sediments from the southern Angola Basin, site 530. Deep Sea Drill.
742 Proj. Init. Rep. 75, 651–655.
743 Schouten, S., Hopmans, E.C., Schefuß, E., Sinninghe Damsté, J.S., 2002. Distributional
744 variations in marine crenarchaeotal membrane lipids: a new tool for reconstructing
745 ancient sea water temperatures? Earth Planet. Sci. Lett. 204 (1-2), 265–274, doi:
746 10.1016/S0012-821X(02)00979-2.
747 Schouten, S., Hopmans E.C., Sinninghe Damsté J.S., 2013. The organic geochemistry of
748 glycerol dialkyl glycerol tetraether lipids: A review. Org. Geochem. 54, 19–61.
749 Sgarrella, F., Di Donato, V., Sprovieri, R., 2012. Benthic foraminiferal assemblage turnover
750 during intensification of the Northern Hemisphere glaciation in the Piacenzian Punta
751 Piccola section. Palaeogeogr. Palaeoclimatol. Palaeoecol. 333–334, 59–74, doi:
752 10.1016/j.palaeo.2012.03.009.
753 Sprovieri, R., Sprovieri, M., Caruso, A., Pelosi, N., Bonomo, S., Ferraro, L., 2006.
754 Astronomic forcing on the planktonic foraminifera assemblage in the Piacenzian Punta
755 Piccola section (southern Italy). Paleoceanography 21 (4), PA4204,
756 doi:10.1029/2006PA001268.

Stratford, K., Williams, R.G., Myers, P.G., 2000. Impact of the circulation on sapropel formation in the eastern Mediterranean. Glob. Biogeochem. Cycles 14 (2), 683–695, doi: 10.1029/1999GB001157.

Tang, C.M., Stott, L.D., 1993. Seasonal salinity changes during Mediterranean sapropel deposition 9 000 years B.P.: Evidence from isotopic analyses of individual planktonic foraminifera. Paleoceanography 8 (4), 473–493, doi: 10.1029/93PA01319.

Van Os, B.J.H., Lourens, L.J., Hilgen, F.J., De Lange, G.J., 1994. The formation of Pliocene sapropels and carbonate cycles in the Mediterranean: diagenesis, dilution, and productivity. Paleoceanography 9 (4), 601–617, doi: 10.1029/94PA00597.

Versteegh, G.J.M., Bosch, H.J., De Leeuw, J.W., 1997. Potential palaeoenvironmental information of C_{24} to C_{36} mid-chain diols, keto-ols and mid-chain hydroxy fatty acids; a critical review. Org. Geochem. 27 (1-2), 1–13, doi: 10.1016/s0146-6380(97)00063-6.

Weijers, J.W.H., Schouten, S., Spaargaren, O.C., Sinninghe Damsté, J.S., 2006. Occurrence and distribution of tetraether membrane lipids in soils: Implications for the use of the TEX_{86} proxy and the BIT index. Org. Geochem. 37 (12), 1680–1693, doi: 10.1016/j.orggeochem.2006.07.018.

Weijers, J. W. H., Schouten, S., Schefuß, E., Schneider, R.R., Sinninghe Damsté, J.S., 2009. Disentangling marine, soil and plant organic carbon contributions to continental margin sediments: A multiproxy approach in a 20,000 year sediment record from the Congo deep-sea fan. Geochim. Cosmochim. Acta 73, 119–132, doi:10.1016/j.gca. 2008.10.016.

Young, J.R., Bown, P.R., 1997. Cenozoic calcareous nannoplankton classification. J. Nannoplankton Res. 19, 36–47.

Figure captions

Figure 1. Geographic position and schematic log of the Punta Grande and Punta Piccola sections. Ages (Lourens et al., 1996) and lithological cycles (Hilgen, 1991) are reported. Planktic foraminifera and calcareous nannofossil biozones are after Cita (1975) and Rio et al. (1990) respectively. The evolution in sedimentation rates (cm/kyr) throughout the studied time interval is also indicated. The picture shows sapropel layers S101-S112 outcropping at Punta Piccola.

Figure 2. Calcareous nannofossil, total organic carbon (TOC) and lipid-biomarker contents during the late Pliocene of Punta Grande/Punta Piccola composite section. **(a)** Total calcareous nannofossil accumulation rate (specimen/cm^2/yr); **(b)** ratio (%) between oligotrophic and mesotrophic calcareous nannofossils; accumulation rates of **(c)** TOC (g/cm^2/yr); **(d)** phytoplanktonic biomarkers (alkenones and diols) (ng/cm^2/yr); and **(e)** glycerol dialkyl glycerol tetraethers (GDGTs) (ng/cm^2/yr). Grey-shaded bands indicate sapropels studied in the present work (S101-S112 and A3-A5).

Figure 3. Variations in the relative proportions (%) of $MeC_{37:2}$ + $MeC_{37:3}$, $EtC_{38:2}$ and $EtC_{39:2}$ alkenones at Punta Grande/Punta Piccola composite section. Profiles 1 and 2 are examples of partial gas-chromatograms. Almost all the studied samples show a similar alkenone distribution (Profile 1), except sapropels S102, S107 and S112 characterized by a distinct alkenone distribution with higher proportions of $EtC_{38:2}$ and $EtC_{39:2}$ alkenones (Profile 2). Profiles 1 and 2 were obtained after $NaBH_4$ reduction of alkenones to alkenols (see text), allowing the detection of EtC_{40}, EtC_{41} and MeC_{41} alkenones.

Figure 4. Reconstructed sea water temperatures during the late Pliocene of Punta Grande/Punta Piccola composite section. Sea temperatures are derived from **(a)** the alkenone

proxy $U^{K'}_{37}$ (eq. 2), **(b)** the long-chain diol index (LDI; eq. 4), and **(c)** the tetraether index TEX_{86} (eq. 6). Colored-bands represent the error range of temperature estimates for each proxy, including analytical and calibration errors. Note that the temperature scale for TEX_{86} (sub)surface temperatures is different from that of $U^{K'}_{37}$ and LDI SSTs.

Figure 5. Comparison between **(a)** oligotrophic relative to mesotrophic calcareous nannofossil data (this study), and **(b)** planktonic and **(c)** benthic foraminifera data (from Sprovieri et al., 2006; Sgarrella et al., 2012) during the late Pliocene of Punta Grande/Punta Piccola composite section.

Figure 6. Data attesting for higher freshwater input during the deposition of sapropels S101-S112. **(a)** The large discrepancies between TEX_{86} and $U^{K'}_{37}$ temperature values observed between 3.1 and 2.8 Ma are likely explained by higher continental inputs during this interval, as attested by **(b)** higher proportions of (terrestrial) branched GDGTs and **(c)** the diol index indicating brackish-freshwater conditions. Our data are in agreement with **(d)** the studies of Foucault and Mélières (2000) and Combourieu Nebout et al. (2004), who evidenced enhanced precipitation and continental runoff during the deposition of sapropels S104-108 based on Palygorskite-Smectie-Chlorite mineral proportions (%) and *Prasynophyceae* pollen concentrations (grains/g sed).

Figure 7. Schematic representations of the environmental conditions and the mechanisms responsible for the formation of sapropels S101-S112 and A4-A5 during the late Pliocene of Punta Grande/Punta Piccola composite section. **(a)** The time interval before 3.1 Ma is characterized by rather low export productivity, with short periods of enhanced productivity. **(b)** Oligotrophic conditions within the photic zone prevailed between 3.1 and 2.8 Ma whereas

832 **(d)** an increase in primary productivity is recorded after 2.8 Ma. **(c)** A strong stratification of
833 the sea water column enhanced organic matter preservation yielding to the formation of
834 sapropels S101-S112. **(e)** Sapropels A4-A5 were formed thanks to enhanced primary
835 productivity in a weakly-stratified water column.
836
837 **Plate 1.** Plate showing the overall good preservation of calcareous nannofossils in sapropel
838 (S) and non-sapropel (NS) layers. **(a-b)** Sample PP36 (18.15 m); **(c-d)** Sample PP35 (17.52
839 m; S102); **(e-g)** Sample PP54 (22.55 m; S107); **(h-i)** Sample PP57 (23.16 m).

Highlights

We discuss the formation of Pliocene sapropels in Sicily using a multi-proxy approach

Recorded increases in SST indicate that sapropels were formed under warmer conditions

Biomarkers/nannofossils show distinct trophic conditions for two sapropel series

The first is due to better organic matter preservation and thermohaline stratification

The second is due to enhanced productivity in a weakly-stratified water column

Figure 1 revised

Click here to download Figure: Fig 1 revised LR.eps

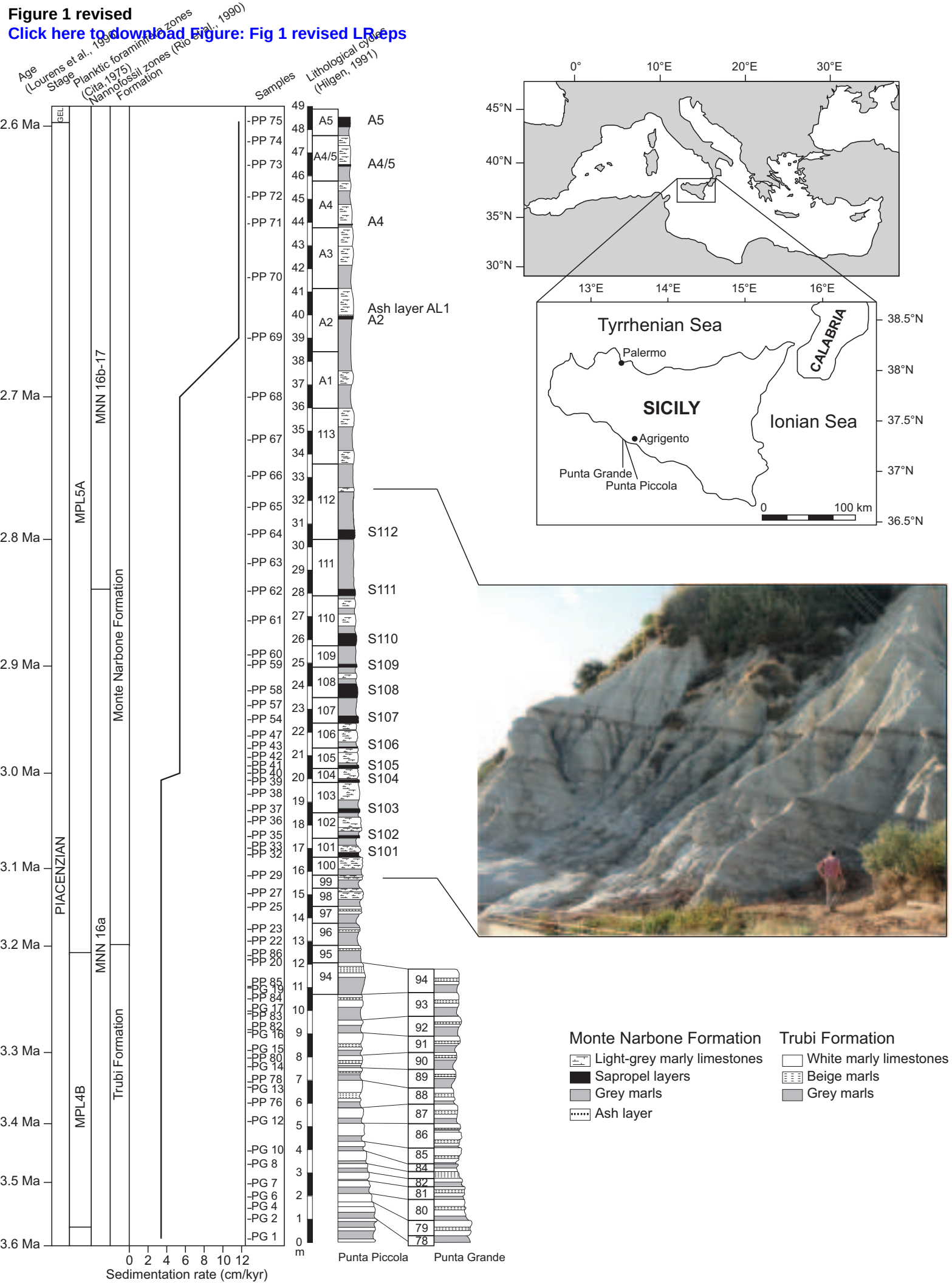

Figure 2 revised

Click here to download Figure: Fig 2 revised.eps

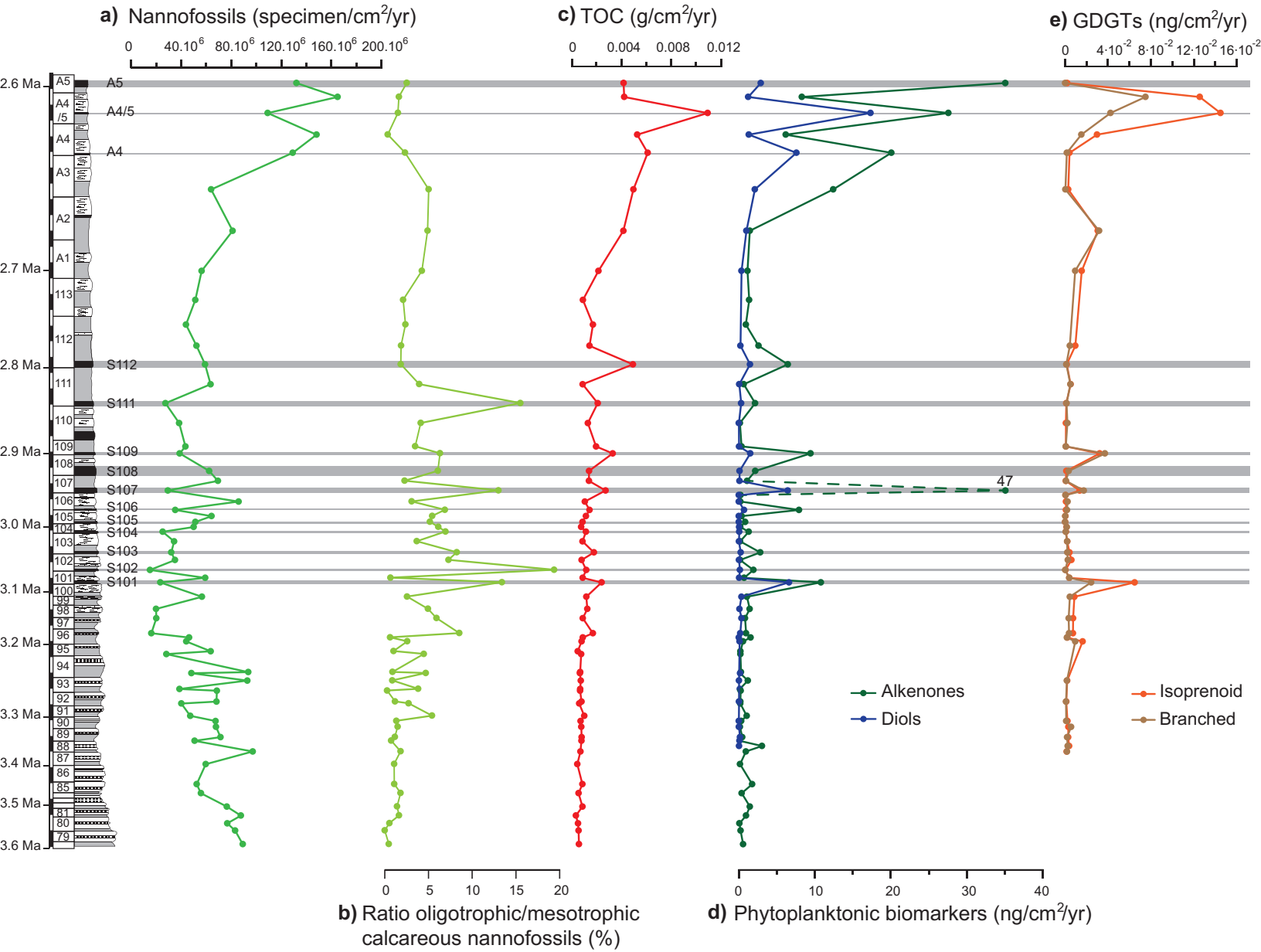

Figure 3 revised

Click here to download Figure: Fig 3 revised.eps

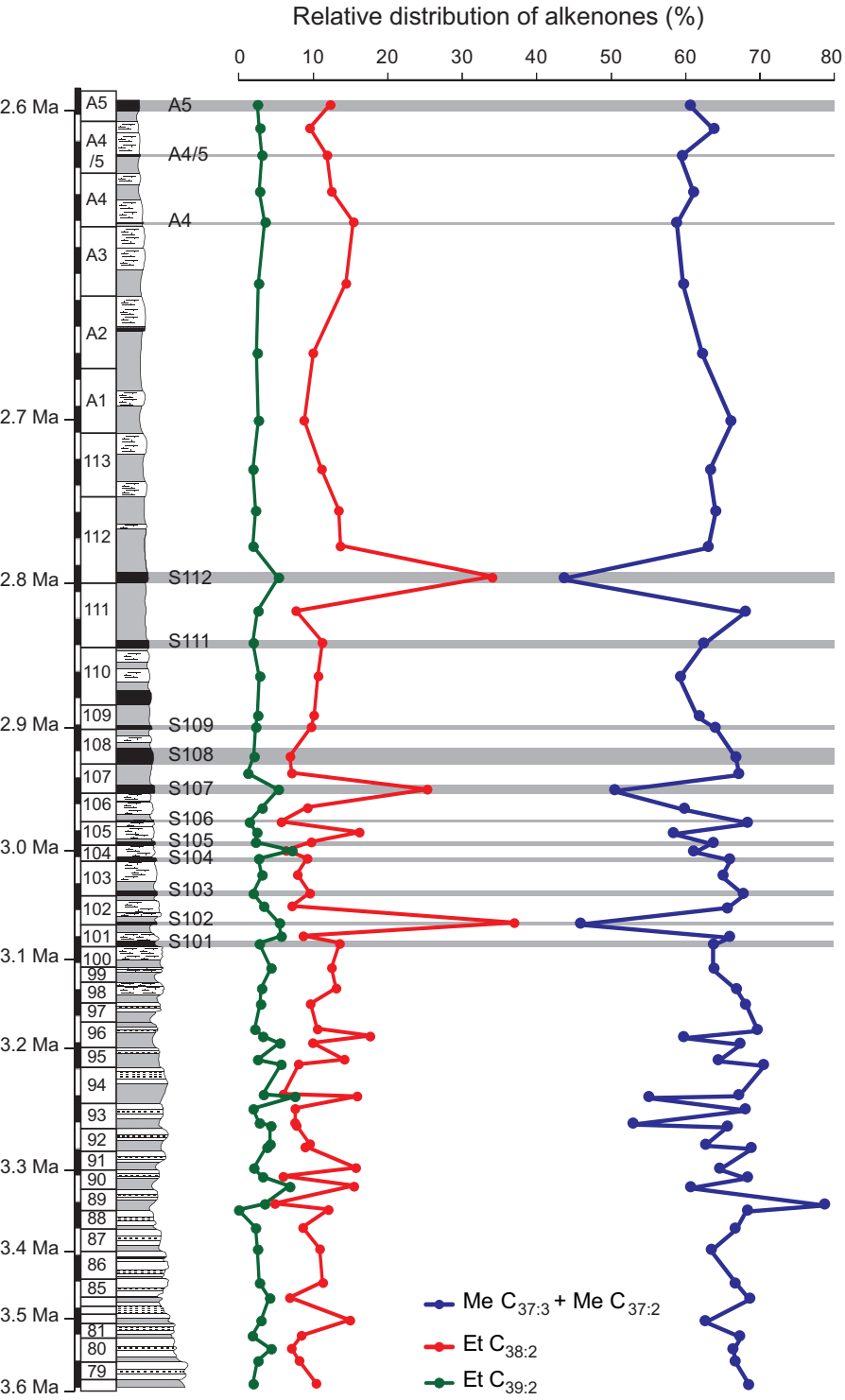

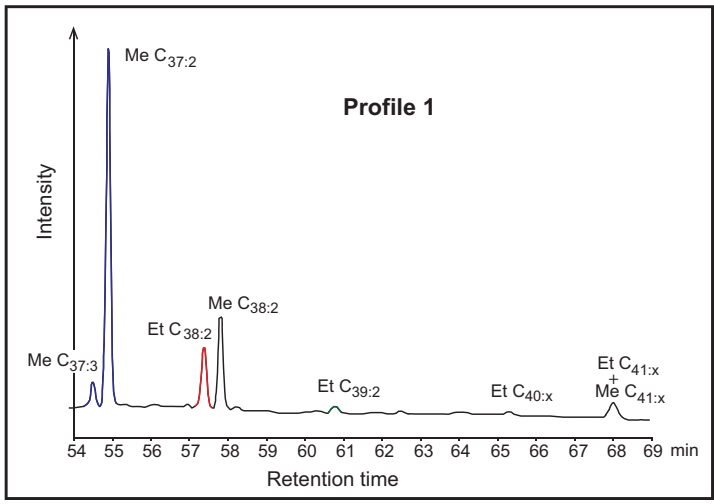

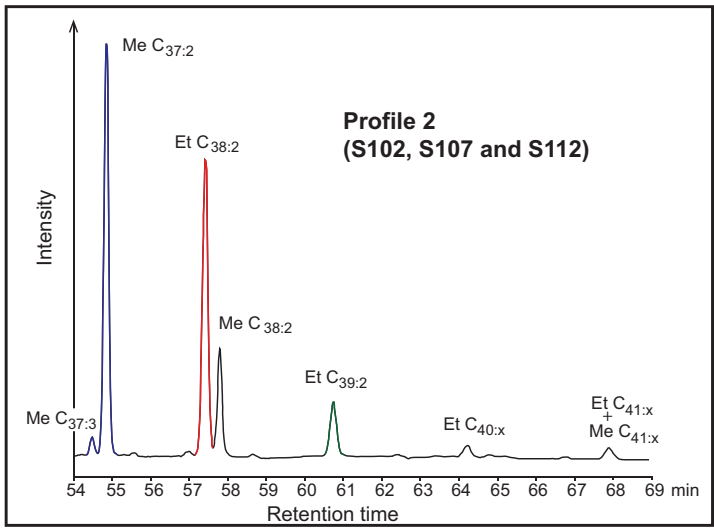

Figure 4 revised

Click here to download Figure: Fig 4 revised.eps

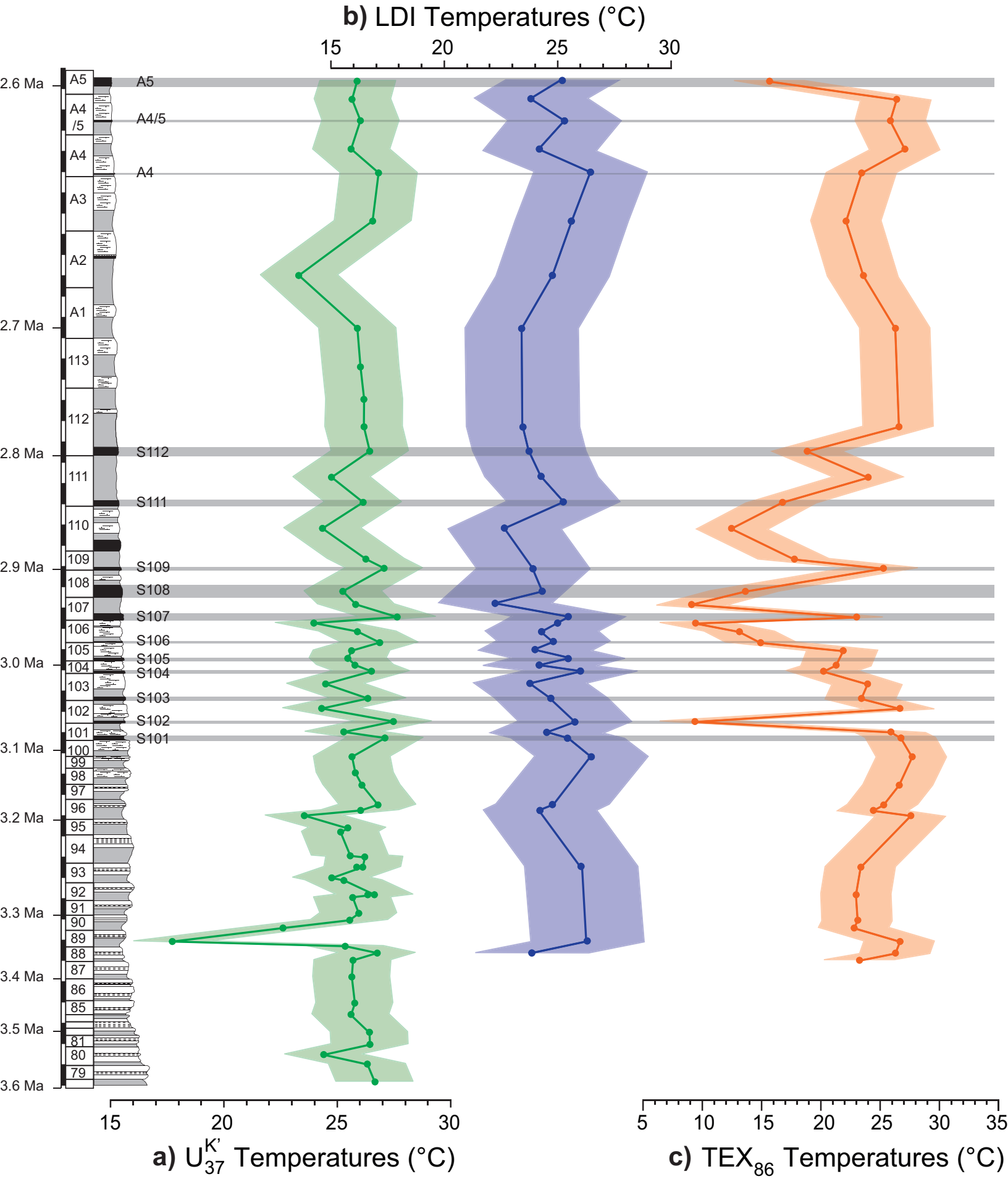

Figure 5 revised

Click here to download Figure: Fig 5 revised.eps

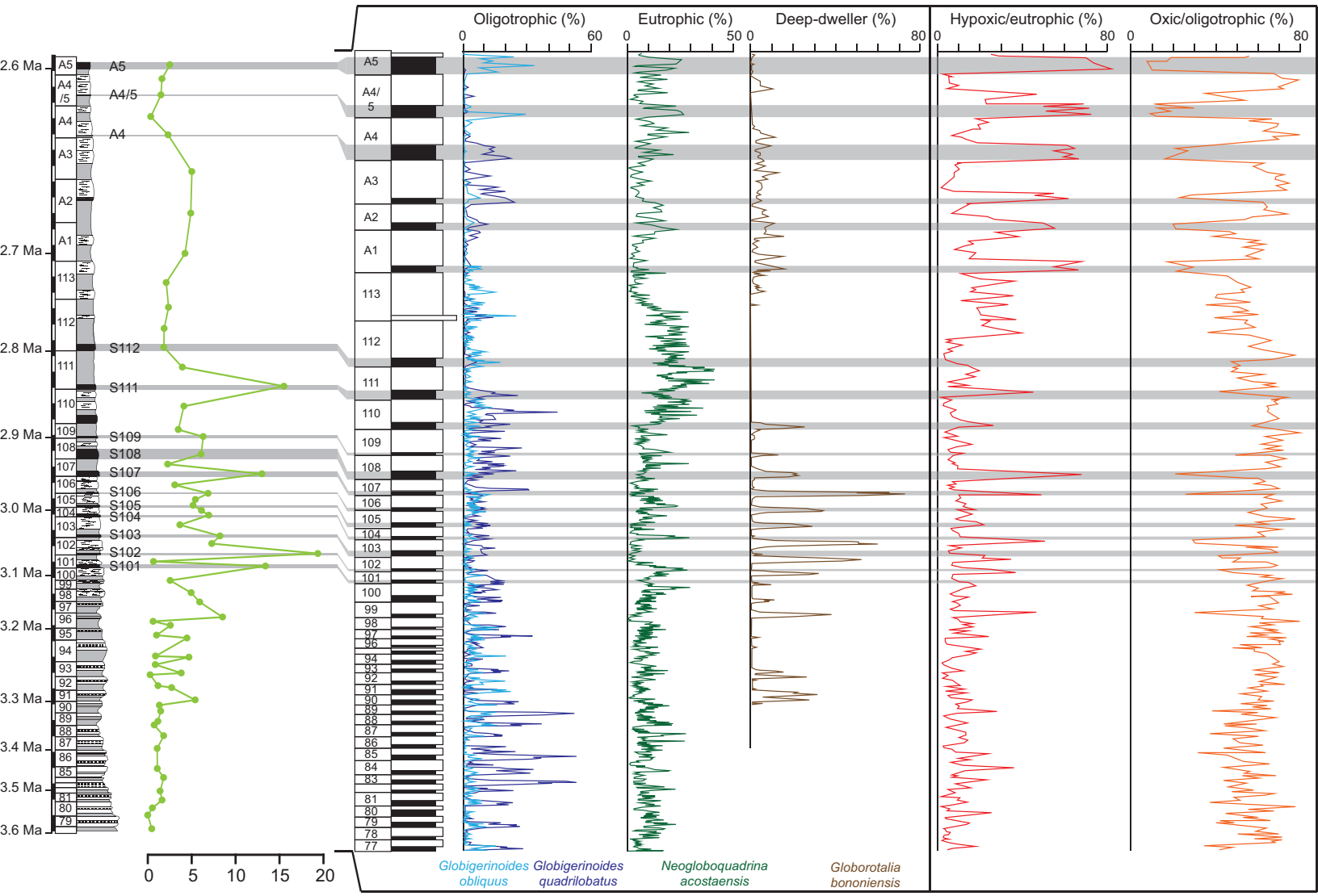

a) Ratio oligotrophic/mesotrophic calcareous nannofossils (%)

b) Planktonic foraminifera (data from Sprovieri et al., 2006)

c) Benthic foraminifera (data from Sgarrella et al., 2012)

Figure 6 revised

Click here to download Figure: Fig 6 revised.eps

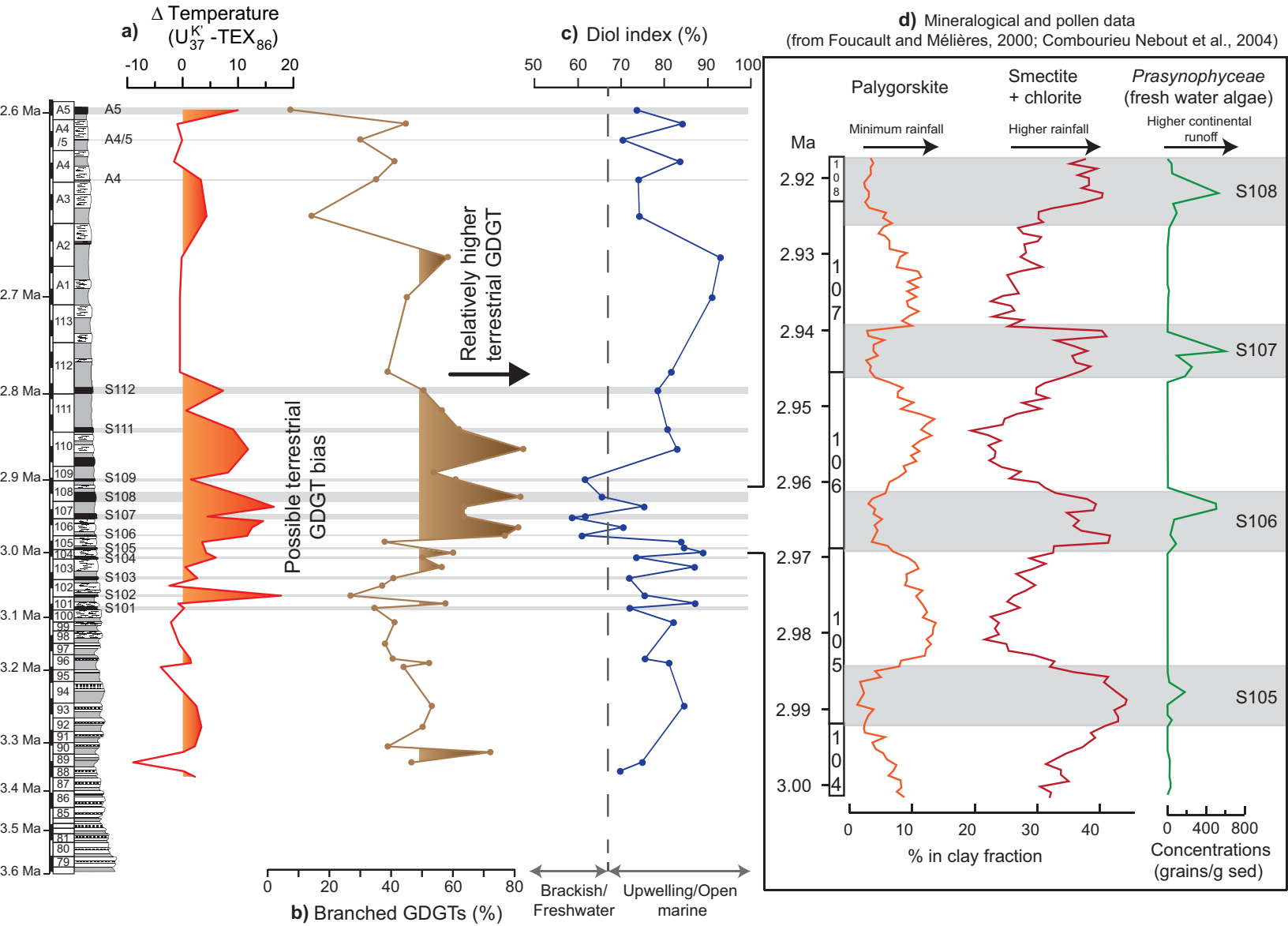

Figure 7 revised

Click here to download Figure: Fig 7 revised LR.eps

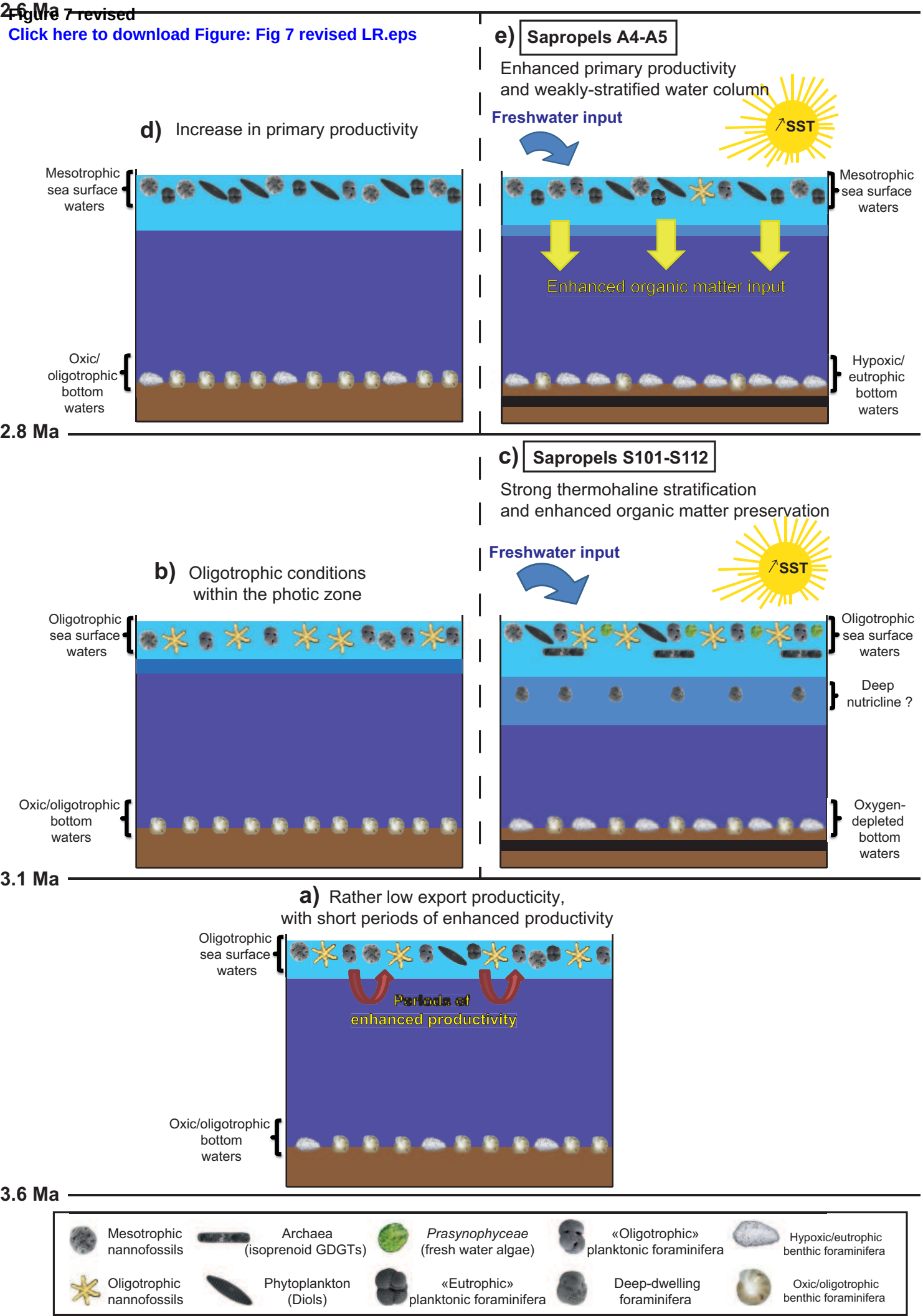

Plate 1 revised

Click here to download Figure: Plate 1.eps-LR.eps

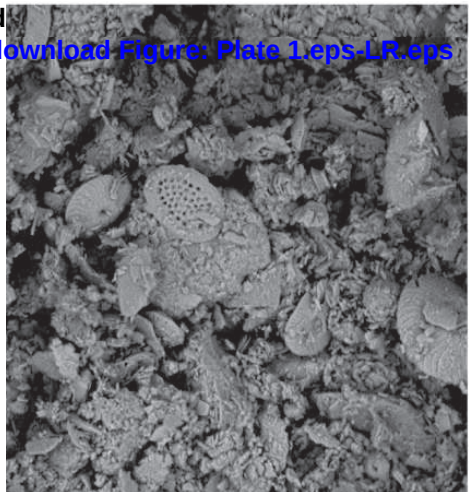

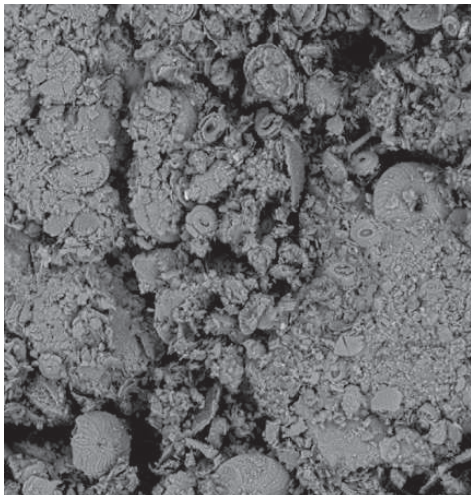

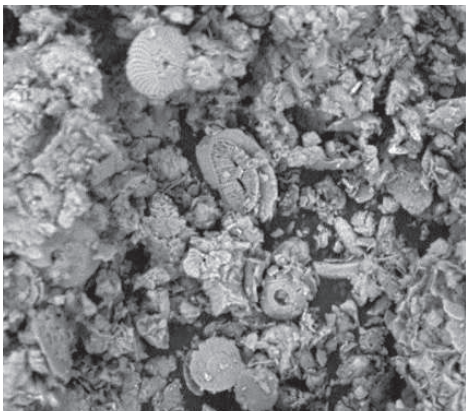

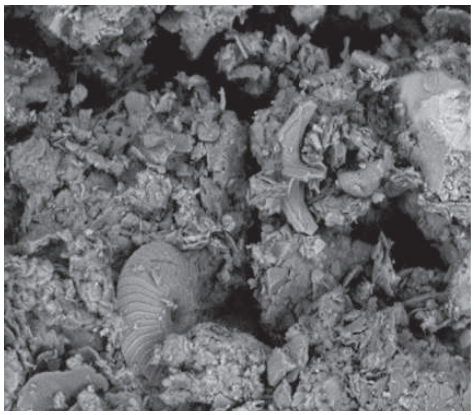

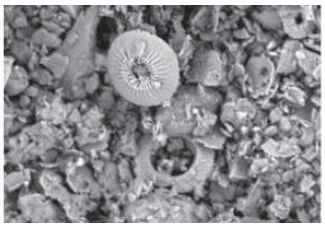

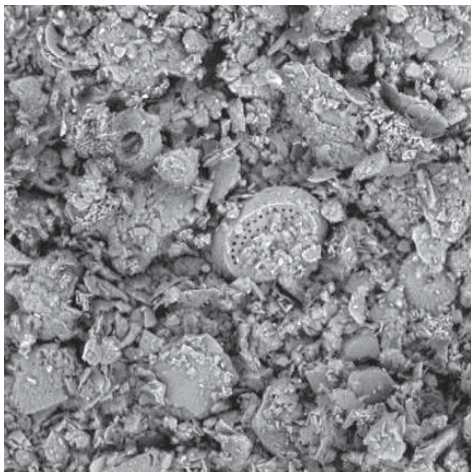

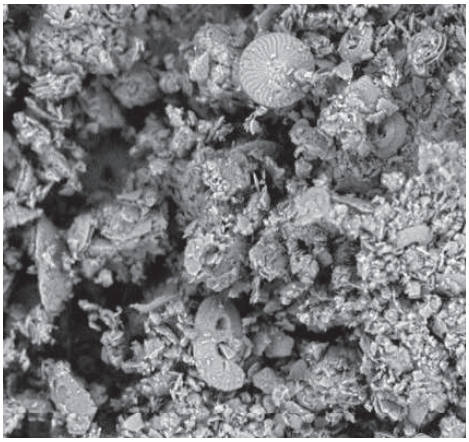

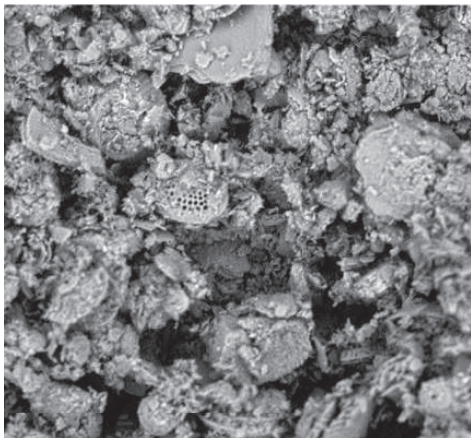

Supplementary information revised

Click here to download Supplementary material for online publication only: Supplementary information revised.docx

Supplementary figure S1

Click here to download Supplementary material for online publication only: Fig S1.eps.eps

Supplementary figure S2

Click here to download Supplementary material for online publication only: Fig S2.eps.eps

Data file

Click here to download Supplementary material for online publication only: Table S1-Data.xlsx